International Journal of Sciences: Basic and Applied Research (IJSBAR)

ISSN 2307-4531
(Print & Online)

http://gssrr.org/index.php?journal=JournalOfBasicAndApplied

Modeling of Tsunami Generation and Propagation by a Spreading Seismic Faulting in two Orthogonal Directions in Linearized Shallow-Water Wave Theory

Khaled T. Ramadan [a]*, Allam. A. Allam [b], M. A. Omar [c]

[a,b,c] *Department of Basic and Applied Science, College of Engineering and Technology, Arab Academy for Science, Technology and Maritime Transport, P.O.BOX 1029, Abu Quir Campus, Alexandria, Egypt.*

Abstract

The process of tsunami evolution during its generation in search for possible amplification mechanisms resulting from spreading of the sea floor uplift in the x-and y-direction is investigated under the effect of rupture velocities, uplift length and width and rise times. This study shows that focusing and amplification of tsunami amplitudes can occur in an arbitrary direction, determined by the velocities of spreading. Tsunami waveforms within the frame of the linearized shallow water theory for constant water depth are analyzed analytically by transform methods (Laplace in time and Fourier in space) for the spreading source model. We analyzed the normalized peak amplitude as a function of the propagated uplift length, width and the average depth of the ocean along the generation path. The amplification of tsunami amplitudes builds up progressively as time increases during the generation process due to wave focusing while the maximum wave amplitude decreases with time during the propagation process due to the geometric spreading and also due to dispersion. The normalized peak amplitudes were smaller when the slip-fault spreads in two orthogonal directions than the numerical values for one dimensional solution because of the interaction of the velocities. The maximum amplitude amplification is proportion to the propagation length and the width of the source model and inversely proportional with the water depth.

Keywords:Tsunami modeling; Shallow water theory; Bottom topography; Water waves; Laplace and Fourier transforms.

---

* Corresponding author.
E-mail address: kramadan@aast.edu

1. Introduction

Shallow water waves, or equivalently, long gravity waves are the waves occurring on the free surface of a fluid and play an important role in a variety of natural phenomena. In contrast to deep water waves, the wavelengths of the

shallow water waves are much longer than the water depth. For these reason, the propagation of these waves is strongly influenced by the shape of the bottom, see [1]. One representative example is tsunami waves.The investigation of the tsunami waves has become of great practical interest that attracts nowadays a lot of attention due in part to the intensive human activity in coastal areas. The evaluation of a local tsunami threat is useful to get a more effective measure for tsunami warning systems and for protection works.There are different natural phenomena that can lead to a tsunami, for example submarine slumps, slides, volcanic explosions, earthquakes, etc.

The massive destruction and loss of life associated with recent tsunamis (Indonesia, 2004; Papua New Guinea, 1998) has underscored the need to develop and implement tsunami hazard mitigation measures. In recent years, significant advances have been made in developing mathematical models to describe the entire process of generation and propagation of a tsunami event generated by seismic seafloor deformation caused by an underwater earthquake.

The sea bottom deformation following an underwater earthquake is a complex phenomenon. This is why, for theoretical or experimental studies, researchers have often used simplified bottom motions such as the vertical motion of a box. Most investigations of tsunami generation and propagation used integral solution (in space and time) for an arbitrary bed displacement spreading based on a linearized description of wave motion in either a two- or three-dimensional fluid domain of uniform depth . The complexity of the integral solutions developed from the linear theory even for the simplest model of bed deformation prevented many authors from determining detailed wave behavior, especially near the source region . However, we construct a three-dimensional source model involved in the transform methods spreading in the $x-$ and $y-$directions that generates a tsunami near the source region.

Many authors have used different analytical solutions and numerical computations to determine the general wave pattern near and far from the source region for a variety of bed motions in a two-or three-dimensional fluid domain.[2] calculated the two-dimensional radiation pattern from a moving source using linear theory.[3] solved the linear long-wave equation in the presence of a moving bottom and a uniformly sloping beach. [4] investigated analytically the generation of tsunamis by submarine slides. They specialized the general solution of the one-dimensional Cauchy linear problem for long water waves to deal with rigid body to explore the characteristics of the generated waves. They studied the body motion in terms of Froude number, wave pattern, wave amplitude and wave energy. [5] studied the generation of long wave through the ocean by a moving bottom. They demonstrated the differences between the classical approach (passive generation) and the active generation under the effect of the bottom motion.

[6] constructed a numerical model of tsunami generation and propagation depending on a nonlinear theory under the effect of a variable bed displacement with constant water depth. They considered nonlinearities and omitted the linear effects of frequency dispersion.

[7] studied theoretically the generated waves by multiplying the static deformations caused by slip along a fault by various time laws: instantaneous, exponential, trigonometric and linear.

[8] performed a comparison between three-dimensional linear and nonlinear tsunami generation models. They observed very good agreement from the superposition of the wave profiles computed with the linear and fully nonlinear models. In addition, they found that the nonlinear shallow water model was not sufficient to model some of the waves generated by a moving bottom because of the presence of frequency dispersion. Moreover, they suggested that for most events the linear theory is sufficient.

[9] discussed the solution of the non-linear problem of propagation of waves generated in a homogeneous fluid, occupying an infinite channel, by the bounded motion of the bottom.He demonstrated that the predictions of the linear theory are in good agreement with those of the nonlinear theory for sufficiently small amplitude of the bottom's motion.

[10] investigated the tsunami evolution during its generation under the effect of the variable velocities of realistic submarine landslides based on a two-dimensional curvilinear slide model. They described the tsunami generation from submarine gravity mass flows in three stages: The first stage represented by a rapid curvilinear down and uplift faulting with rise time. The second stage represented by a unilaterally propagation in the positive direction to a significant length to produce curvilinear two-dimensional models represented by a depression slump, and a displaced accumulation slide model. The last stage represented by the time variation in the velocity of the accumulation slide (block slide) by using transforms method.

[11] studied the nature of the tsunami build up and propagation during and after realistic curvilinear source models represented by a slowly uplift faulting and a spreading slip-fault model. They studied the tsunami amplitude amplification as a function of the spreading velocity and rise time. They also analyzed the normalized peak amplitude as a function of the propagated uplift length, width and the average depth of the ocean.

Previous studies for tsunami generation considered only one-dimensional movement of kinematic source models. For example, [12] studied experimentally the generated waves by raising or lowering a box at one end of a channel. He considered two types of time histories: an exponential and a half-sine bed movement.[13] investigated the generation of waves by a slowly spreading uplift of the bottom in linearized shallow-water wave theory. They showed that the effects of the spreading of the ocean floor deformation (faulting, submarine slides or slumps) on the amplitudes and periods of the generated tsunamis are largest when the spreading velocity of uplift and the tsunami velocity are comparable.[14] mentioned the source parameters for submarine slides and earthquakes including source duration, displacement amplitude, areas and volumes of selected past earthquakes that have or may have generated a tsunami. They contributed the nature of tsunami sources to create tsunami waveforms in the near field and provided a starting point for their elementary mathematical model.[15]

investigated tsunami generation by a slowly spreading uplift of the sea floor in the near field considering the effects of the source finiteness and directivity. They described mathematically various two-dimensional kinematic models of submarine slumps and slides as combinations of spreading constant or slopping uplift functions.There results show that for given constant water depth, the peak amplitude depends on the ratio of the spreading velocity of the sea floor to the long wavelength tsunami velocity, see [16].

[17] and [18] determined the tsunami amplitudes caused by submarine land slumps and slides spreading in two orthogonal directions. All the previous approach mentioned above computed tsunami waveforms using linearized shallow water theory and transform methods of solution. We follow the same approach but with a more complex source model represented by a sliding Heaviside step function in two orthogonal directions. We demonstrated the waveform amplification resulting from the two dimensional source spreading and wave focusing in the near-field and the tsunami spreading in the far-field. In this paper we investigate the tsunami generation and propagation under the effect of various paraments of a seismic faulting source model spreading in two orthogonal directions following an underwater earthquake. This problem is a more extended and generalized problem and more sophisticated than one-dimensional problems. This model resembles the initial source predicted according to the initial disturbance recorded in [19] and [20]. We discuss aspects of tsunami generation that should be considered in developing these model, as well as the propagation wave after the formation of the source models have been completed.

We study the fluid wave motion above finite source, with variable distribution of the ocean floor uplift, for variable spreading velocities. Here we aim to demonstrate the large scale tsunami generation features computed during the formation of the tsunami source for different ratios between the velocities of the source propagation and the tsunami speed, as well as the overall propagation following the source. Comparison between our results and others obtained for the tsunami model in the near -field is done. According to the results and the numerical estimation, we analyze the normalized peak amplitude as a function of the characteristics size of the source model and the water depth.

2. Mathematical Formulation of the Problem

Consider a three dimensional fluid domain Ω as shown in Figure 1. It is supposed to represent the ocean above the fault area. It is bounded above by the free surface of the ocean $z = \eta(x, y, t)$ and below by the rigid ocean floor $z = -h(x, y) + \zeta(x, y, t)$, where $\eta(x, y, t)$ is the free surface elevation, $h(x, y)$ is the water depth and $\zeta(x, y, t)$ is the sea floor displacement function. The domain Ω is unbounded in the horizontal directions x and y, and can be written as $\Omega = R^2 \times [-h(x, y) + \zeta(x, y, t), \eta(x, y, t)]$. For simplicity, $h(x, y)$ is assumed to be a constant. Before the earthquake, the fluid is assumed to be at rest, thus the free surface and the solid boundary are defined by $z = 0$ and $z = -h$, respectively. Mathematically, these conditions can be written in the form of initial conditions: $\eta(x, y, 0) = \zeta(x, y, 0) = 0$. At time $t > 0$, the bottom boundary moves in a prescribed manner which is given by $z = -h + \zeta(x, y, t)$. The deformation of the sea bottom is assumed to have all the necessary properties needed to compute its Fourier transform in x, y and its Laplace transform in t. The resulting deformation of the free surface $z = \eta(x, y, t)$ is to be found as part of the solution. It is assumed that the fluid is incompressible and the flow is irrotational. The former implies the existence of a velocity potential $\Phi(x, y, z, t)$

which fully describes the flow and the physical process. By definition of Φ, the fluid velocity vector can be expressed as $\vec{q} = \nabla\Phi$. Thus, the potential flow $\Phi(x, y, z, t)$ must satisfy the Laplace's equation

$$\nabla^2\Phi(x, y, z, t) = 0 \qquad \text{where} \qquad (x, y, z) \in \Omega\,, \tag{1}$$

The potential $\Phi(x, y, z, t)$ must satisfy the following kinematic and dynamic boundary conditions on the free surface and the solid boundary, respectively:

$$\Phi_z = \eta_t + \Phi_x\eta_x + \Phi_y\eta_y \qquad \text{on} \qquad z = \eta(x, y, t)\,, \tag{2}$$

$$\Phi_z = \zeta_t + \Phi_x\zeta_x + \Phi_y\zeta_y \qquad \text{on} \qquad z = -h + \zeta(x, y, t)\,, \tag{3}$$

and

$$\Phi_t + \frac{1}{2}(\nabla\Phi)^2 + g\ \eta = 0 \qquad \text{on} \qquad z = \zeta(x, y, t)\,. \tag{4}$$

where g is the acceleration due to gravity. As described above, the initial conditions are given by

(5)

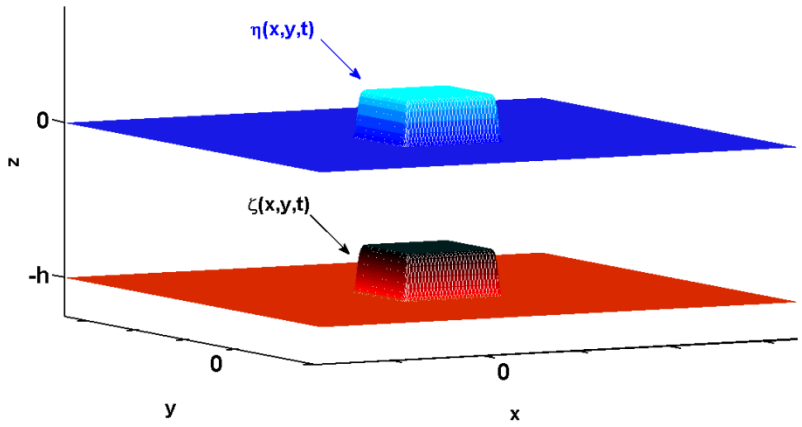

Figure 1: Definition of the fluid domain and coordinate system for a very rapid movement of the assumed source model.

2.1 Linear Shallow Water Theory

Various approximations can be considered for the full water-wave equations. One is the system of Boussinesq equations that retains nonlinearity and dispersion up to a certain order. Boussinesq model is used to study transient varying bottom problems. [21] and [22] presented a developed numerical model based on the highly accurate Boussinesq-type formulation subjected to exact expressions for the kinematic and dynamic free surface conditions. Their results show that the model was capable of treating the full life cycle of tsunami evolution, from the initial generation of bottom movements, to the subsequent propagation, and through the final run-up

process. Reasonable computational efficiency has been demonstrated in their work, which made the model attractive for practical coastal engineering studies, where high dispersive and nonlinear accuracy is sought. Another one is the system of nonlinear shallow-water equations that retains nonlinearity but no dispersion. Solving this problem is a difficult task due to the nonlinearities and the a priori unknown free surface. The concept of shallow water is based on the smallness of the ratio between water depth and wave length. In the case of tsunamis propagating on the surface of deep oceans, one can consider that shallow-water theory is appropriate because the water depth (typically several kilometers) is much smaller than the wave length (typically several hundred kilometers), which is reasonable and usually true for most tsunamis triggered by submarine earthquakes, slumps and slides, see [7] and [12]. Hence, the problem can be linearized by neglecting the nonlinear terms in the boundary conditions (2) - (4) and applying the boundary conditions on the nondeformed instead of the deformed boundary surfaces (i.e. $\mathbf{z} = -\mathbf{h}$ and on $\mathbf{z} = \mathbf{0}$ instead of $\mathbf{z} = -\mathbf{h} + \boldsymbol{\zeta}(\mathbf{x}, \mathbf{y}, \mathbf{t})$ and $\mathbf{z} = \boldsymbol{\eta}(\mathbf{x}, \mathbf{y}, \mathbf{t})$). The linearized problem in dimensional variables can be written as

$$\nabla^2 \Phi(x, y, z, t) = 0 \text{ where } (x, y, z) \in R^2 \times [-h, 0], \qquad (6)$$

subjected to the following boundary conditions

$$\Phi_z = \eta_t \qquad \text{on } z = 0, \qquad (7)$$

$$\Phi_z = \zeta_t \qquad \text{on } z = -h, \qquad (8)$$

$$\Phi_t + g\,\eta = 0 \quad \text{on } z = 0, \qquad (9)$$

The linearized shallow water solution can be obtained by the Fourier-Laplace transform.

2.2 Solution of the Problem

Our interest is the resulting uplift of the free surface elevation $\eta(x, y, t)$. An analytical analysis is examine to illustrate the generation and propagation of a tsunami for a given bed profile $\zeta(x, y, t)$. Mathematical modeling of waves generated by vertical and lateral displacements of submarine slide and slump using the combined Fourier-Laplace transform of the Laplace equation analytically is the simplest way of studying tsunami development. All our studies were taken into account constant depths for which the Laplace and Fast Fourier Transform (FFT) methods could be applied. The equations (6 - 9) can be solved by using the method of integral transforms. We apply the Fourier transform in (x, y)

$$\mathcal{F}_{xy}\{f(x,y)\} = f^{**}(k_1, k_2) = \int_{-\infty}^{\infty} \int_{-\infty}^{\infty} e^{-i(k_1 x + k_2 y)} f(x,y)\, dx\, dy,$$

with its inverse transform

$$\mathcal{F}^{-1}_{k_1 k_2}\{f^{**}(k_1, k_2)\} = f(x,y) = \frac{1}{(2\pi)^2} \int_{-\infty}^{\infty} \int_{-\infty}^{\infty} e^{i(x k_1 + y k_2)} f^{**}(k_1, k_2)\, dk_1\, dk_2,$$

and the Laplace transform in time t is defined as

$$\mathcal{L}\{g(t)\} = \hat{g}(s) = \int_0^{\infty} e^{-st}\, g(t)\, dt\,.$$

Combining (7) and (9) yields the single free-surface condition

$$\Phi_{tt}(x, y, 0, t) + g\ \Phi_z(x, y, 0, t) = 0\,. \tag{10}$$

After applying the transforms and using the property $\left[\mathcal{F}\left\{\frac{d^n f}{dx^n}\right\} = (i\,k)^n f^*(k)\right]$ and the initial conditions (5), Equations (6), (8) and (10) become,

$$\hat{\Phi}^{**}_{zz}(k_1, k_2, z, s) - (k_1^2 + k_2^2)\hat{\Phi}^{**}(k_1, k_2, z, s) = 0\,, \tag{11}$$

$$\hat{\Phi}^{**}_{z}(k_1, k_2, -h, s) = s\,\hat{\zeta}^{**}(k_1, k_2, s)\,, \tag{12}$$

$$s^2\hat{\Phi}^{**}(k_1, k_2, 0, s) + g\ \hat{\Phi}^{**}_{z}(k_1, k_2, 0, s) = 0\,. \tag{13}$$

The transformed free-surface elevation can be obtained from (9) as

$$\hat{\eta}^{**}(k_1, k_2, s) = -\frac{s}{g}\hat{\Phi}^{**}(k_1, k_2, 0, s) = 0\,. \tag{14}$$

A general solution of (11) will be given by

$$\hat{\Phi}^{**}(k_1, k_2, z, s) = A(k_1, k_2, s)\cosh(k\,z) + B(k_1, k_2, s)\sinh(k\,z)\,. \tag{15}$$

where $k = \sqrt{k_1^2 + k_2^2}$. The functions $A(k_1, k_2, s)$ and $B(k_1, k_2, s)$ can be easily found from the boundary conditions (12) and (13):

$$A(k_1, k_2, s)\cosh(k\,z) = -\frac{g\ s\,\hat{\zeta}^{**}(k_1,k_2,s)}{\cosh(k\,h)\,[s^2 + g\ k\tanh(k\,h)]}\,, \tag{16}$$

$$B(k_1, k_2, s)\cosh(k\,z) = \frac{s^3\hat{\zeta}^{**}(k_1,k_2,s)}{k\cosh(k\,h)\,[s^2 + g\ k\tanh(k\,h)]}\,. \tag{17}$$

Substituting (16,17) in the general solution (15) yields

$$\hat{\Phi}^{**}(k_1, k_2, z, s) = -\frac{g\ s\,\hat{\zeta}^{**}(k_1,k_2,s)}{\cosh(k\,h)\,(s^2+\omega^2)}\left(\cosh(k\,z) - \frac{s^2}{g\ k}\sinh(k\,z)\right). \tag{18}$$

where $\omega = \sqrt{g\ k\tanh(k\,h)}$ is the circular frequency of the wave motion. The free surface elevation $\eta^{**}(k_1, k_2, s)$ can be obtained from (14) as

$$\hat{\eta}^{**}(k_1, k_2, s) = \frac{s^2\hat{\zeta}^{**}(k_1,k_2,s)}{(s^2+\omega^2)\cosh(kh)}\,, \tag{19}$$

The circular frequency ω describes the dispersion relation of tsunamis and implies phase velocity $c = \frac{\omega}{k}$ and group velocity $U = \frac{d\omega}{dk}$. Hence, $c = \sqrt{\frac{g \tan h(kh)}{k}}$, and $U = \frac{1}{2}\, c \left(1 + \frac{2kh}{\sin h(2kh)}\right)$. Since, $k = \frac{2\pi}{\lambda}$,hence as $kh \to 0$, both $c \to \sqrt{gh}$ and $U \to \sqrt{gh}$, which implies that the tsunami velocity $v_t = \sqrt{gh}$ for wavelengths λ long compared to the water depth h. The free surface elevation $\eta(x, y, t)$ can be evaluated for a specified $\zeta(x, y, t)$ by obtaining its transform $\hat{\zeta}^{**}(k_1, k_2, s)$, then substituting it into (19) and inverting $\hat{\eta}^{**}(k_1, k_2, s)$ analytically to obtain $\eta^{**}(k_1, k_2, t)$ which is further converted to $\eta(x, y, t)$ by using double inverse Fourier Transform. The above linearized solution is known as the shallow water solution.

The free surface elevation $\eta^{**}(k_1, k_2, t)$ can be evaluated by using inverse Laplace transform of $\eta^{**}(k_1, k_2, s)$ from the Convolution theorem as follows

$$\eta^{**}(k_1, k_2, t) = \frac{1}{\cos h(kh)}\left[\zeta^{**}(k_1, k_2, t) - \omega \int_0^t \sin(\omega(t-u))\, \zeta^{**}(k_1, k_2, u)\, du\right], \tag{20}$$

The sea floor displacement is taken as

$$\zeta(x, y, t) = \zeta_0\, H\left(t - \frac{x}{v_1}\right)\, H\left(t - \frac{y}{v_2}\right), \tag{21}$$

where H(x) represents the Heaviside function and ζ_0 denotes the initial uplift of the bottom topography. Fourier transform can now be applied to the bottom topography (21) to obtain

$$\begin{aligned}
\zeta^{**}(k_1, k_2, t) &= \zeta_0 \left(\int_0^{L_1} e^{-ik_1 x}\, H\left(t - \frac{x}{v_1}\right) dx\right)\left(\int_0^{L_2} e^{-ik_2 y}\, H\left(t - \frac{y}{v_2}\right) dy\right) \\
&= \zeta_0 \left(\begin{cases} \int_0^{tv_1} e^{-ik_1 x}\, dx, & \text{for} \quad t \le t_1^* \\ \int_0^{L_1} e^{-ik_1 x}\, dx, & \text{for} \quad t > t_1^* \end{cases}\right)\left(\begin{cases} \int_0^{tv_2} e^{-ik_2 y}\, dy, & \text{for} \quad t \le t_2^* \\ \int_0^{L_2} e^{-ik_2 y}\, dy, & \text{for} \quad t > t_2^* \end{cases}\right) \\
&= \zeta_0 \left(\frac{-1}{k_1 k_2}\right)\left(\begin{cases} \left(1 - e^{-ik_1 v_1 t}\right), & \text{for} \quad t \le t_1^* \\ \left(1 - e^{-ik_1 L_1}\right), & \text{for} \quad t > t_1^* \end{cases}\right)\left(\begin{cases} \left(1 - e^{-ik_2 v_2 t}\right), & \text{for} \quad t \le t_2^* \\ \left(1 - e^{-ik_2 L_2}\right), & \text{for} \quad t > t_2^* \end{cases}\right) \\
&= \zeta_0 \left(\frac{-1}{k_1 k_2}\right) \begin{cases} \left(1 - e^{-ik_1 v_1 t}\right)\left(1 - e^{-ik_2 v_2 t}\right), & \text{for} \quad t \le t_1^* \quad \text{and} \quad t \le t_2^* \\ \left(1 - e^{-ik_1 v_1 t}\right)\left(1 - e^{-ik_2 L_2}\right), & \text{for} \quad t \le t_1^* \quad \text{and} \quad t > t_2^* \\ \left(1 - e^{-ik_1 L_1}\right)\left(1 - e^{-ik_2 v_2 t}\right), & \text{for} \quad t > t_1^* \quad \text{and} \quad t \le t_2^* \\ \left(1 - e^{-ik_1 L_1}\right)\left(1 - e^{-ik_2 L_2}\right), & \text{for} \quad t > t_1^* \quad \text{and} \quad t > t_2^* \end{cases} \\
&= \zeta_0 \left(\frac{-1}{k_1 k_2}\right) \sum_{i=1}^{4} I_i(k_1, k_2, t)
\end{aligned} \tag{22}$$

where $t_1^* = \frac{L_1}{v_1}$ and $t_2^* = \frac{L_2}{v_2}$, L_1 and L_2 represents the propagated uplift length and width, v_1 and v_2 denoted the rupture velocities of the slip fault in the $x-$ and $y-$ direction respectively and

$$\begin{aligned} I_1(k_1,k_2,t) &= I_{11}(k_1,k_2,t)\, H(t_1^*-t)\, H(t_2^*-t) \\ I_2(k_1,k_2,t) &= I_{21}(k_1,k_2,t)\, H(t_1^*-t)\, H(t-t_2^*) \\ I_3(k_1,k_2,t) &= I_{31}(k_1,k_2,t)\, H(t-t_1^*)\, H(t_2^*-t) \\ I_4(k_1,k_2,t) &= I_{41}(k_1,k_2,t)\, H(t-t_1^*)\, H(t-t_2^*) \end{aligned} \tag{23}$$

and

$$\begin{aligned} I_{11}(k_1,k_2,t) &= \left(1-e^{-ik_1v_1t}\right)\left(1-e^{-ik_2v_2t}\right) \\ I_{21}(k_1,k_2,t) &= \left(1-e^{-ik_1v_1t}\right)\left(1-e^{-ik_2L_2}\right) \\ I_{31}(k_1,k_2,t) &= \left(1-e^{-ik_1L_1}\right)\left(1-e^{-ik_2v_2t}\right) \\ I_{41}(k_1,k_2,t) &= \left(1-e^{-ik_1L_1}\right)\left(1-e^{-ik_2L_2}\right) \end{aligned} \tag{24}$$

Substituting (22) into the integral of (20), we obtain

$$\int_0^t \sin(\omega(t-u))\, \zeta^{**}(k_1,k_2,u)\, du = \zeta_0 \left(\frac{-1}{k_1k_2}\right) \sum_{i=1}^{4} \int_0^t \sin(\omega(t-u))\, I_i(k_1,k_2,u)\, du \tag{25}$$

where

$$\int_0^t \sin(\omega(t-u))\, I_1(k_1,k_2,u)\, du = \int_0^{\min(t,t_1^*,t_2^*)} \sin(\omega(t-u))\, I_{11}(k_1,k_2,u)\, du \tag{26}$$

$$\int_0^t \sin(\omega(t-u))\, I_2(k_1,k_2,u)\, du = \int_{t_2^*}^{\min(t,t_1^*)} \sin(\omega(t-u))\, I_{21}(k_1,k_2,u)\, du \tag{27}$$

$$\int_0^t \sin(\omega(t-u))\, I_3(k_1,k_2,u)\, du = \int_{t_1^*}^{\min(t,t_2^*)} \sin(\omega(t-u))\, I_{31}(k_1,k_2,u)\, du \tag{28}$$

$$\int_0^t \sin(\omega(t-u))\, I_4(k_1,k_2,u)\, du = \int_{\max(t_1^*,t_2^*)}^{t} \sin(\omega(t-u))\, I_{41}(k_1,k_2,u)\, du \tag{29}$$

The integral of equation (26) is written as :

$$\begin{aligned} &\int_0^t \sin(\omega(t-u))\, I_1(k_1,k_2,u)\, du = \\ &\frac{\cos(\omega(t-\min(t,t_1^*,t_2^*))) - \cos(\omega t)}{\omega} \\ &- \frac{e^{-\min(t,t_1^*,t_2^*)\, i k_1 v_1}}{\omega^2 - k_1^2 v_1^2} \left(\omega \cos(\omega(\min(t,t_1^*,t_2^*)-t)) + i k_1 v_1 \sin(\omega(\min(t,t_1^*,t_2^*)-t))\right) \\ &- \frac{i k_1 v_1 \sin(\omega t) - \omega \cos(\omega t)}{\omega^2 - k_1^2 v_1^2} \\ &- \frac{e^{-\min(t,t_1^*,t_2^*)\, i k_2 v_2}}{\omega^2 - k_2^2 v_2^2} \left(\omega \cos(\omega(\min(t,t_1^*,t_2^*)-t)) + i k_2 v_2 \sin(\omega(\min(t,t_1^*,t_2^*)-t))\right) \\ &- \frac{i k_2 v_2 \sin(\omega t) - \omega \cos(\omega t)}{\omega^2 - k_2^2 v_2^2} \\ &+ \frac{e^{-\min(t,t_1^*,t_2^*)\, i (k_1 v_1 + k_2 v_2)}}{\omega^2 - (k_1 v_1 + k_2 v_2)^2} \left(\omega \cos(\omega(\min(t,t_1^*,t_2^*)-t)) + i (k_1 v_1 + k_2 v_2) \sin(\omega(\min(t,t_1^*,t_2^*)-t))\right) \\ &+ \frac{i (k_1 v_1 + k_2 v_2) \sin(\omega t) - \omega \cos(\omega t)}{\omega^2 - (k_1 v_1 + k_2 v_2)^2} \end{aligned} \tag{30}$$

The same can be done for equations (27), (28) and (29). The free surface elevation $\eta^{**}(k_1,k_2,t)$ will be given as :

$$\eta^{**}(k_1,k_2,t) = \frac{\zeta_0}{\cos h(kh)}\left(\frac{-1}{k_1 k_2}\right) \quad [\sum_{i=1}^{4} I_i(k_1,k_2,t) - \omega\left(\int_0^{\min(t,t_1^*,t_2^*)} \sin(\omega(t-u))\, I_{11}(k_1,k_2,u)\, du + \int_{t_2^*}^{\min(t,t_1^*)} \sin(\omega(t-u))\, I_{21}(k_1,k_2,u)\, du + \int_{t_1^*}^{\min(t,t_2^*)} \sin(\omega(t-u))\, I_{31}(k_1,k_2,u)\, du + \int_{\max(t_1^*,t_2^*)}^{t} \sin(\omega(t-u))\, I_{41}(k_1,k_2,u)\, du\right)\Big] \tag{31}$$

This completes the solution of the problem, $\eta^{**}(k_1,k_2,t)$, in the double Fourier transform domain.

Finally, $\eta(x,y,t)$ is evaluated using the inverse fast Fourier transform (IFFT). The IFFT is a fast algorithm for efficient implementation of the Inverse Discrete Fourier Transform (IDFT). In this paper, this inversion is done using the Matlab IFFT algorithm.

In order to implement the algorithm efficiently, singularities should be removed by finite limits as follows:

1. As $k \to 0$, implies $k_1 \to 0$, $k_2 \to 0$ and $\omega \to 0$, then $\eta^{**}(k_1,k_2,t)$ has the following limit:

$$\lim_{k\to 0}\eta^{**}(k_1,k_2,t) = \zeta_0\,(v_1 v_2)\,\zeta^{**}(k_1,k_2,t)|_{k=0}$$

where

$$\zeta^{**}(k_1,k_2,t)|_{k=0} = t^2\,H(t_1^*-t)\,H(t_2^*-t) + t\,t_2^*\,H(t_1^*-t)\,H(t-t_2^*) + t_1^*\,t\,H(t-t_1^*)\,H(t_2^*-t) + t_1^* t_2^*\,H(t-t_1^*)\,H(t-t_2^*)$$

2. As $k_1 \to 0$, implies $k = k_2$ and $\omega = \sqrt{g\,k_2\tanh(k_2 h)}$, then $\eta^{**}(k_1,k_2,t)$ has the following limit:

$$\lim_{k\to 0}\eta^{**}(k_1,k_2,t) = \frac{1}{\cos h(k_2 h)}\left[\zeta^{**}(k_1,k_2,t)|_{k_1=0} - \omega\int_0^t \sin(\omega(t-u))\,\zeta^{**}(k_1,k_2,u)|_{k_1=0}\, du\right] \tag{32}$$

where

$$\zeta^{**}(k_1,k_2,t)|_{k_1=0} = \zeta_0\frac{v_1}{ik_2}\Big[t\left(1-e^{-ik_2 v_2 t}\right)H(t_1^*-t)\,H(t_2^*-t) + t\left(1-e^{-ik_2 L_2}\right)H(t_1^*-t)\,H(t-t_2^*) + t_1^*\left(1-e^{-ik_2 v_2 t}\right)H(t-t_1^*)\,H(t_2^*-t) + t_1^*\left(1-e^{-ik_2 L_2}\right)H(t-t_1^*)\,H(t-t_2^*)\Big] \tag{33}$$

and

$$\begin{aligned}\int_0^t\uparrow \sin(\omega(t-u)) \quad & \zeta^{**}(k_1,k_2,u)|_{k_1=0}\,du \\ &= \zeta_0\frac{v_1}{ik_2}\Big[\int_0^{\min(t,t_1^*,t_2^*)}\uparrow \sin(\omega(t-u))\,u\left(1-e^{-ik_2v_2u}\right)du \\ &\quad+\int_{t_2^*}^{\min(t,t_1^*)}\uparrow \sin(\omega(t-u))\,u\left(1-e^{-ik_2L_2}\right)du \\ &\quad+\int_{t_1^*}^{\min(t,t_2^*)}\uparrow \sin(\omega(t-u))\,t_1^*\left(1-e^{-ik_2v_2u}\right)du \\ &\quad+\int_{\max(t_1^*,t_2^*)}^{t}\uparrow \sin(\omega(t-u))\,t_1^*\left(1-e^{-ik_2L_2}\right)du\Big]\end{aligned} \tag{34}$$

3. As $k_2\to 0$, implies $k=k_1$ and $\omega=\sqrt{g\,k_1\tanh(k_1h)}$, then $\eta^{**}(k_1,k_2,t)$ has the following limit:

$$\lim_{k\to 0}\eta^{**}(k_1,k_2,t)=\frac{1}{\cos h\,(k_2h)}\Big[\zeta^{**}(k_1,k_2,t)|_{k_2=0}-\omega\int_0^t\uparrow \sin(\omega(t-u))\,\zeta^{**}(k_1,k_2,u)|_{k_2=0}\,du\Big] \tag{35}$$

where

$$\begin{aligned}\zeta^{**}(k_1,k_2,t)|_{k_2=0}=\zeta_0\frac{v_2}{ik_1}\quad & \Big[t\left(1-e^{-ik_1v_1t}\right)H(t_1^*-t)\,H(t_2^*-t) \\ &+t_2^*\left(1-e^{-ik_1v_1t}\right)H(t_1^*-t)\,H(t-t_2^*) \\ &+t\left(1-e^{-ik_1L_1}\right)H(t-t_1^*)\,H(t_2^*-t) \\ &+t_2^*\left(1-e^{-ik_1L_1}\right)H(t-t_1^*)\,H(t-t_2^*)\Big]\end{aligned} \tag{36}$$

and

$$\begin{aligned}\int_0^t\uparrow \sin(\omega(t-u)) \quad & \zeta^{**}(k_1,k_2,u)|_{k_2=0}\,du \\ &= \zeta_0\frac{v_2}{ik_1}\Big[\int_0^{\min(t,t_1^*,t_2^*)}\uparrow \sin(\omega(t-u))\,u\left(1-e^{-ik_1v_1u}\right)du \\ &\quad+\int_{t_2^*}^{\min(t,t_1^*)}\uparrow \sin(\omega(t-u))\,t_2^*\left(1-e^{-ik_1v_1u}\right)du \\ &\quad+\int_{t_1^*}^{\min(t,t_2^*)}\uparrow \sin(\omega(t-u))\,u\left(1-e^{-ik_1L_1}\right)du \\ &\quad+\int_{\max(t_1^*,t_2^*)}^{t}\uparrow \sin(\omega(t-u))\,t_2^*\left(1-e^{-ik_1L_1}\right)du\Big]\end{aligned} \tag{37}$$

3. Results and Discussion

In this section, we present numerical results to illustrate the nature of the tsunami build up and propagation during and after the uplift process of the bottom topography spreading in both $x-$ and $y-$directions. This model was used to evaluate tsunami waveforms up to distances of several source dimensions, for various combinations of the model parameters (depth to the sea bed, h, fault length and width, L_1 and L_2, and velocities of rupture propagation along the fault length and width; in the positive $x-$ and $y-$directions with v_1 and v_2, respectively, and time since rupture initiation, t). The numerical results demonstrate the waveform amplification resulting from source spreading in two orthogonal directions and wave focusing in the near-field and the tsunami spreading in the far-field under the effect of different factors.

When the source process is completed and for rapid lateral spreading, the displacement of the free surface above the source resembles the displacement of the ocean floor. For velocities of spreading smaller thanv_t then the tsunami amplitudes in the direction of the source propagation become small with high frequencies. As the

velocity of the spreading approaches v_t, the tsunami waveform has progressively larger amplitude, with high frequency content, in the direction of the slip spreading, see [11] and [13]. These large amplitudes are caused by wave focusing (i.e. during slow earthquakes). Examples of such slow earthquakes are the June 6, 1960, Chile earthquakes which ruptured as a series of earthquakes for about an hour, see [23], and the February 21, 1978, Banda Sea earthquake, see [24].

Tsunami generally occurs due to vertical movement of the seafloor that vertically displaces the water column. Large vertical displacement of the sea bottom ground causes a corresponding large motion at the sea surface. The generation of tsunami by vertical displacements of the ocean floor depends on the characteristic size (length L_1 and width L_2) of the displaced area and on the time t it takes to spread the motion over the entire source region. Horizontal deformation of the sea bottom ground does not cause large changes at the sea surface. Therefore, researchers presented kinematic source models in the form of Heaviside functions to describe the generation of tsunamis, see [12 - 17].

It is difficult to estimate, at present, how often the amplification may occur during actual faulting, sliding or slumping, because of the lack of detailed knowledge about the ground deformations in the source area of past tsunamis. Therefore, we construct mathematically a tsunami source model represented by a sliding Heaviside step function spreading in two orthogonal directions. We first examine the significance of the spreading velocities of the ocean floor uplift by comparing displacement waveforms in 3 −dimensional frame of work for various values of the ratio v_1/v_2.

3.1 Effect of the spreading velocities v_1 and v_2 on tsunami generation waveform

In this section, the focusing and the amplification of the tsunami amplitude, determined by the velocities of spreading is studied. The effect of the spreading velocities on the tsunami generation is illustrated in Figure 2 for spreading length L_1 and spreading width L_2 equal 100 km, and water depth $h = 2$ km at the time when the source process is completed (i.e. at $t = t_2^* = L_2/v_2$) and $v = \sqrt{v_1^2 + v_2^2}$ represents the resultant velocity. It can be observed in Figures 1 and 1 that the case when $v_1 = v_2$ at $t = t_2^* = L_2/v_2$ can be considered a case of symmetric collisions between two waves of equal amplitudes. It is known from [25] that waves in collisions always lose a small amount of amplitude due to the collision even for interactions between large waves in comparable with the case when $v_1 \neq v_2$ as shown in Figures (2c) and (2d). The residual is clearly visible in the Figure (2a) which were in the form of wave trains behind the leading wave. It can be observed from Figure (2b) that the maximum amplification occurs when $v_1 = v_2 = v_t$ at water depth $h = 2$ km which agrees with the work done by [11] and [13] whom verified that the amplification η/ζ_0 is largest when the velocity of the uplift is close to the velocity of the tsunami wave due to wave focusing at the time when the source process is completed. Hence, we chose the case in which the velocities of the sea floor are equal to the long wave tsunami velocity v_t (i.e. maximum amplification) in studying the generation and propagation of the tsunami waveforms.

The amplification shown in Figure 2 depends on the spreading velocities v and the time t taken to spread the motion over the entire source region. This observation can be verified by comparing the result obtained in Figure (2b) with the tsunami waveform obtained by using a kinematic source model represented by a sliding

Heaviside step function spreading in one direction (i.e. neglecting the vertical co-seismic displacement in the $y-$direction and hence it propagates instantaneously). This case was studied by [13]. They considered a square source model characterized by $L_1 = L_2 = 50$ km, with uniform final elevation ζ_0, and the velocity of lateral spreading of the ocean floor uplift was constant. We expand the propagation length L_1 to 100 km and L_2 to 100 km for the Heaviside step function in order to make comparison with the results we obtained.

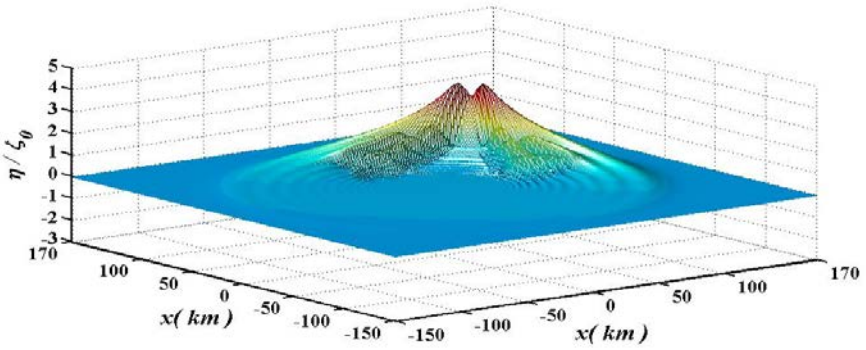

(a) $v_1 = v_2$ and $v = v_t = \sqrt{v_1^2 + v_2^2}$ at $t = t_2^* = \frac{L_2}{v_2}$

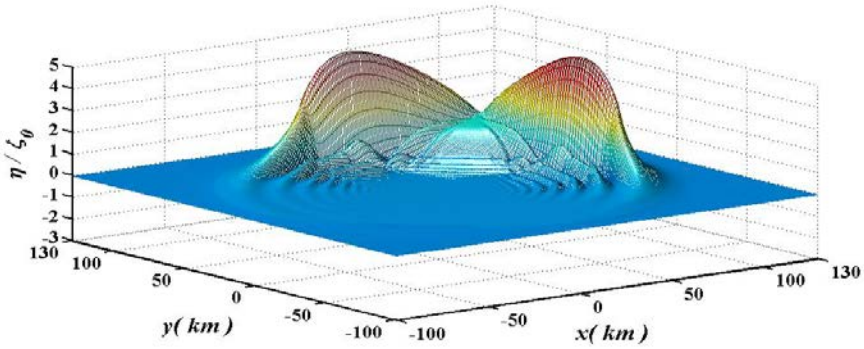

(b) $v_1 = v_2 = v_t$ at $t = t_2^* = \frac{L_2}{v_2}$

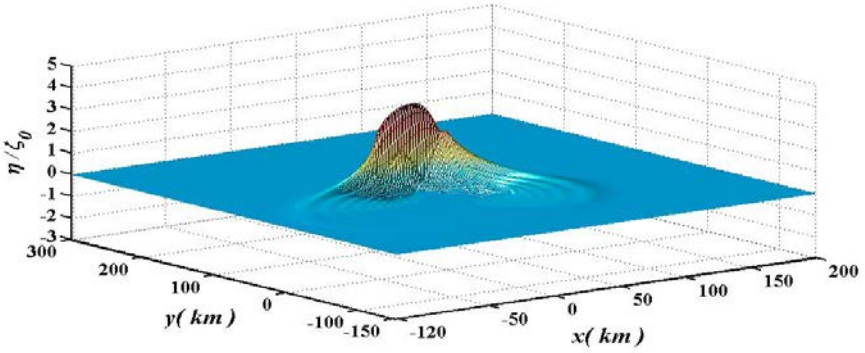

(c) $v_1 = 0.5v_2 \text{and} v = v_t = \sqrt{v_1^2 + v_2^2}$ at $t = t_2^* = \frac{L_2}{v_2}$

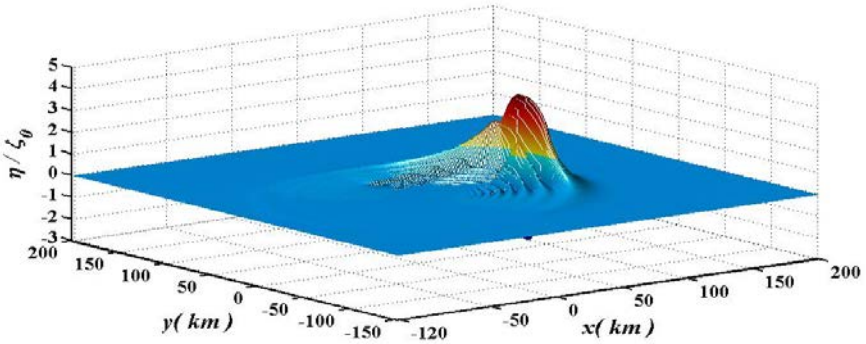

(d) $v_2 = 0.5v_1 \text{and} v = v_t = \sqrt{v_1^2 + v_2^2}$ at $t = t_1^* = \frac{L_1}{v_1}$

Figure 2: The normalized tsunami waveforms η/ζ_0 for different spreading velocities v_1 and v_2 at $L_1 = L_2 =$ 100 km and h = 2 km.

Figure 3 illustrates the cross section from the $y-$direction of the tsunami waveforms generated by the sliding Heaviside step function spreading in two orthogonal directions and the slide model spreading in one direction with $L_1 = 100$ km and $L_2 = 100$ km when the maximum amplitude amplification occurs at $v = v_t$. It can be observed when $v_1 = v_2 = v_t$ obtained normalized peak amplitudes η/ζ_0 smaller than the numerical values for one dimensional solution. This happened because of the interaction of the velocities. The cross section taken either from the $x-$ or $y-$directions is the same for the tsunami waveforms generated by the sliding Heaviside step function spreading in two orthogonal directions when $v_1 = v_2 = v_t$, due to the symmetry in the generation of the free surface elevations.

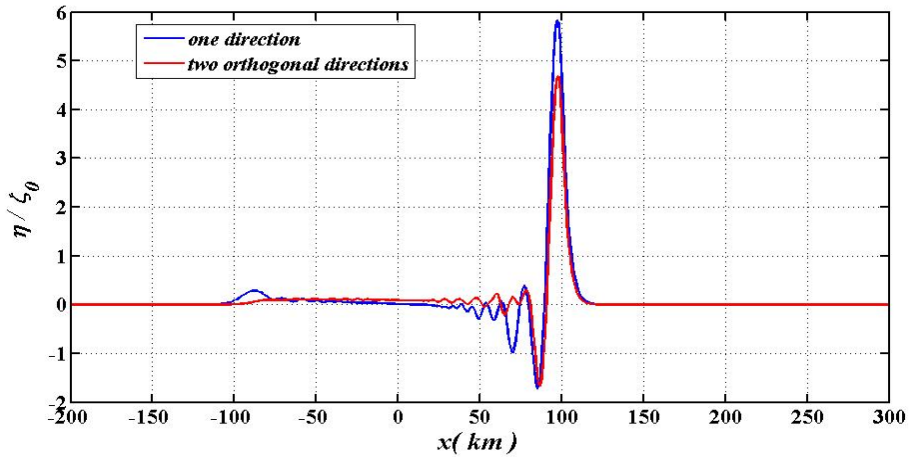

Figure 3: Maximum tsunami amplitude at spreading velocity generated by fault source model spreading in one direction for $v = v_t$ and the fault source model spreading in two orthogonal directions for at $t = t_2^* = L_2/v_2$.

3.2 Tsunami Generation and Propagation-Evolution in Time

The effects of variations of the spreading fault source in two orthogonal movements on the generation and propagation of tsunamis above and away from the considered source model are studied as a function of time t in Figures 4 and 5, respectively. These effects are studied through the investigation of the generation and propagation of tsunamis by movement in the $x-$ and $y-$direction of the seismic faulting under the effect of the characteristic size length L_1 and width L_2 of the displaced area and the water depth h. Previous studies neglected the vertical co-seismic displacement in the $y-$direction and hence it propagates instantaneously, see [13 - 16]. In this study, we considered the spreading of the seismic faulting in two orthogonal directions according to the tsunami event of the 2012 Indian Ocean earthquakes where the rupture of these earthquakes occurred on multiple, almost orthogonal faults and the Was Grand Banks event of 1929 a slump spreading in two directions [17]. The process of tsunami generation and propagation for the spreading fault model in two orthogonal directions is illustrated in Figures 4 and 5, respectively, for $L_1 = L_2 = 100$ km at water depth $h = 2$ km with constant spreading velocities $v_1 = v_2 = v_t$ at time generation $t = 0.25\, t_2^*,\ 0.5\, t_2^*,\ 0.75\, t_2^*$ and t_2^* where $t_2^* = L_2/v_2$ and time propagation $t = 2\, t_2^*,\ 3\, t_2^*,\ 4\, t_2^*$ and $5\, t_2^*$. Figure 6 represents the side view of the waves illustrated in Figures 4 and 5. It can be seen from Figure 4 that the amplitude of the wave builds up progressively in two directions as t increases due to wave focusing. The wave will be focusing and the amplification may occur above the spreading edge of the source model, which can be observed from Figure (6a). This amplification occurs above the source progressively, as the source evolves, by adding uplifted fluid to the fluid displaced previously by uplifts of preceding source segments. As the spreading length and width in the fault increases, the amplitude of the tsunami wave increases. As the wave propagates, the maximum wave amplitude decreases with time due to the geometric spreading and also due to the dispersion causing a train of small waves forms behind the main wave, as shown in Figures 5 and (6b).

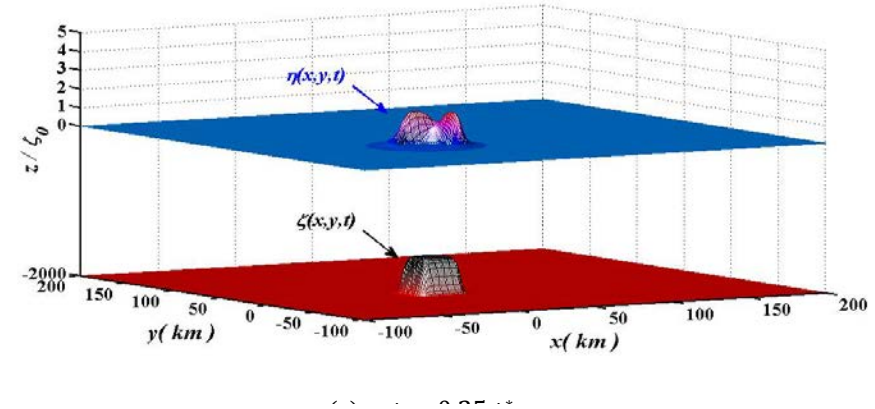

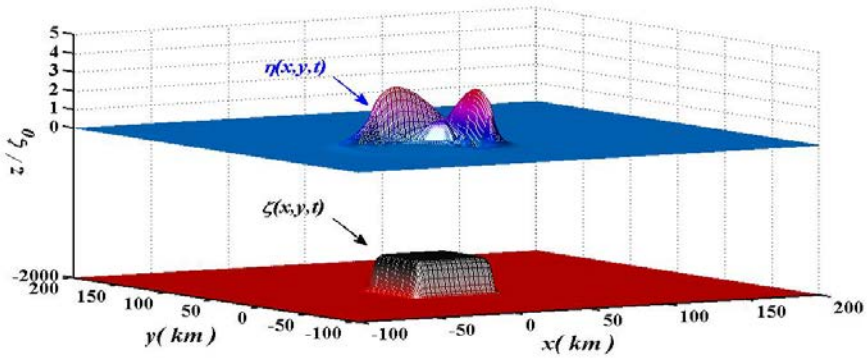

(b) at $t = 0.5\ t_2^*$

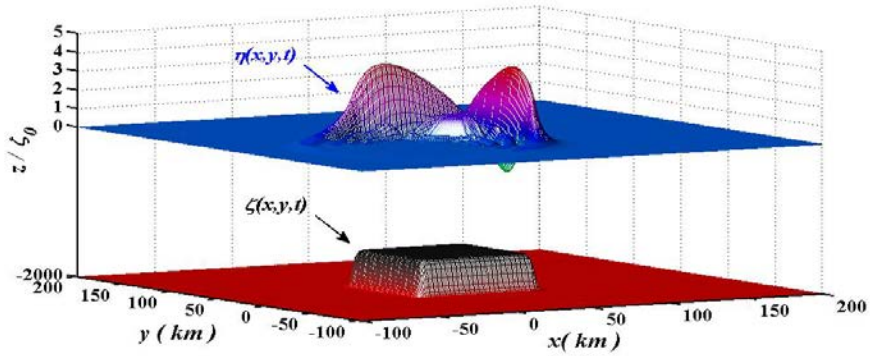

(c) at $t = 0.75\ t_2^*$

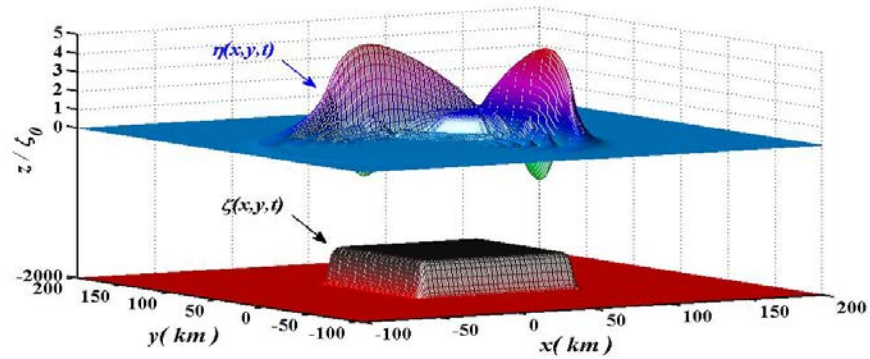

(d) at $t = t_2^*$

Figure 4: 3-dimensional view of tsunami generated waveforms at time $t = 0.25t_2^*, 0.5t_2^*, 0.75t_2^*$ and t_2^*

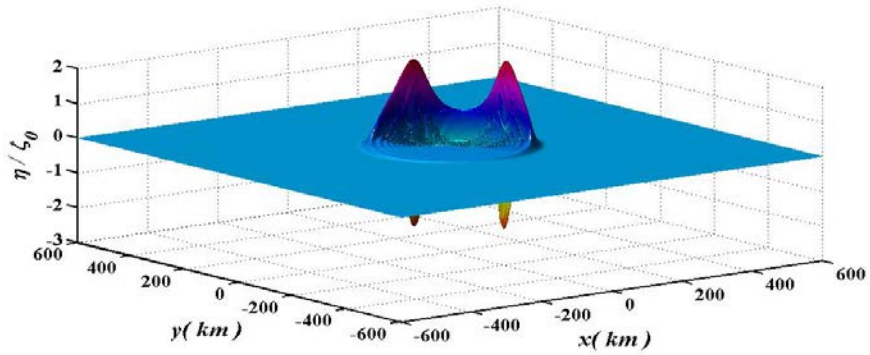

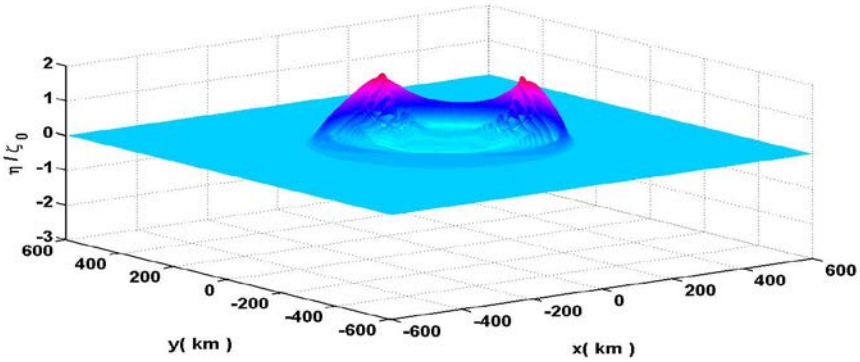

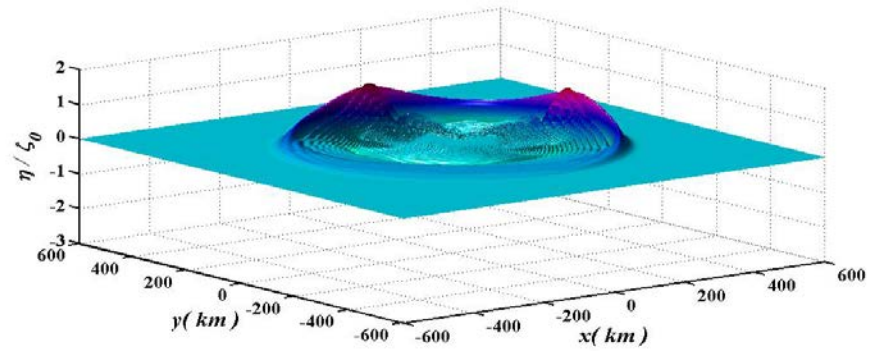

(c) at $t = 4\ t_2^*$

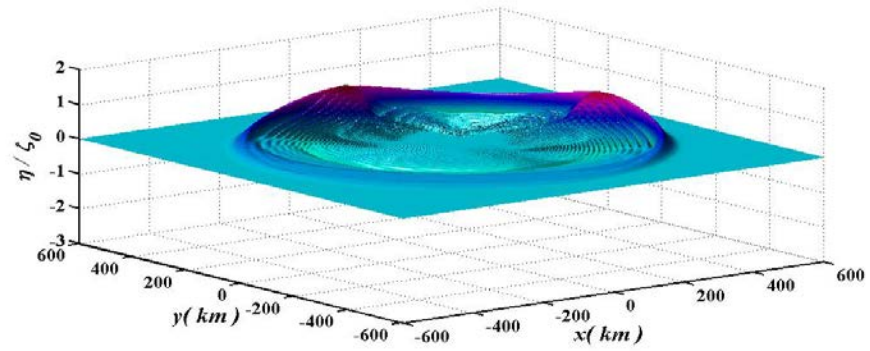

(d) at $t = 5\ t_2^*$

Figure 5: Three-dimensional view of tsunami propagated waveforms at time $t = 2\ t_2^*, 3\ t_2^*, 4\ t_2^*$ and $5t_2^*$

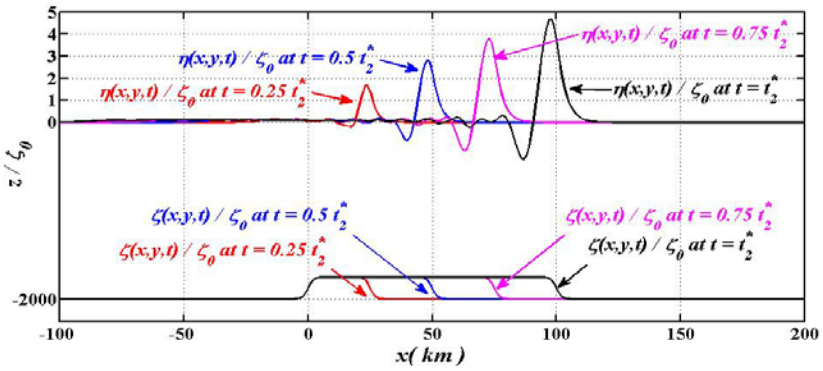

(a) Tsunami generated waveforms

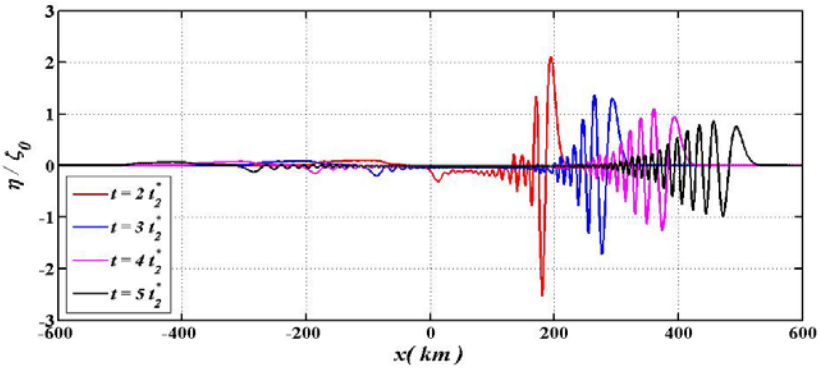

(b) Tsunami propagated waveforms

Figure 6: Side view of tsunami generation and propagated waveforms

3.3 Effect of propagated uplift length L_1 and width L_2 on tsunami generation waveform

The generation of tsunamis by vertical displacements of the ocean floor depends on the characteristic size length L_1 and width L_2 of the displaced area and on the time t over the entire source region as shown in Figure 7. It is seen as the spreading length L_1 and width L_2 in the bottom topography increase, the amplitude of the tsunami waves increases.

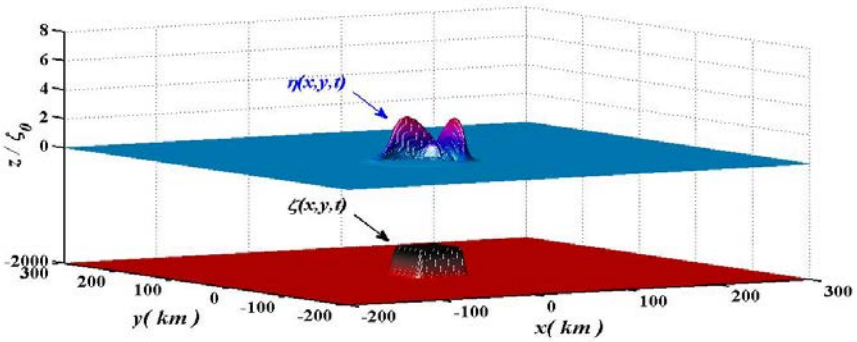

(a) $L_1 \times L_2 = 50 \times 50$

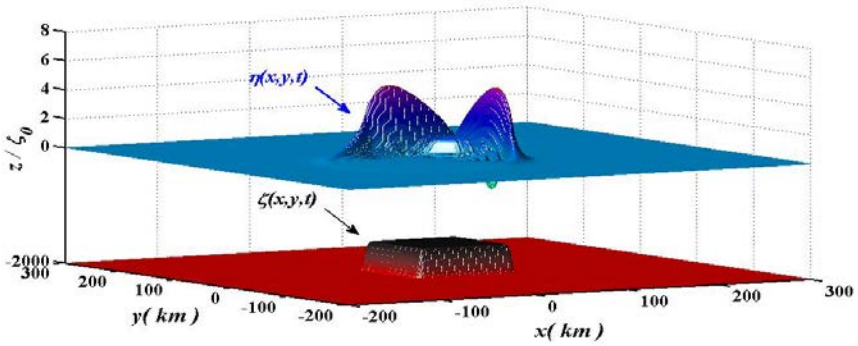

(b) $L_1 \times L_2 = 100 \times 100$

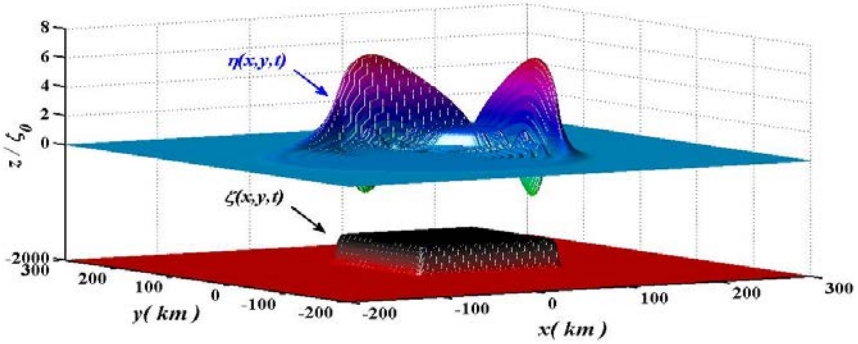

(c) $L_1 \times L_2 = 150 \times 150$

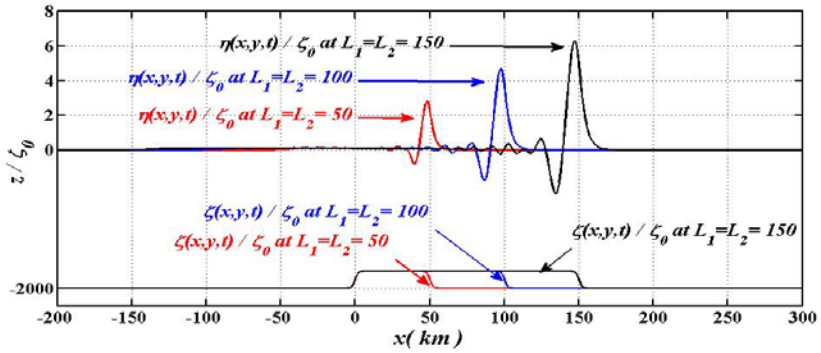

(d) Side view

Figure 7: The normalized tsunami generation waveformsη/ζ_0 at different propagated uplift length L_1 and width$L_2 v_1 = v_2 = v_t$ and $h = 2$ km at $t = t_2^* = L_1/v_t$

Table 1 shows the variation in the amplification factorη_{max}/ζ_0 for various values of the propagated uplift length L_1 and width L_2 at $h = 2$ km and $t = t_1^* = L_1/v_1$. It can be seen from the table that for L_1/h between 5 and 250, varies from 0.3384 to 14.920. It can be observed that the amplification increases with the increase inL_1/h and with the increase in L_2/h. The numerical results obtained in Table 1 agrees with the aspect of the amplification factor of the tsunami waves obtained in [13] which was created by an uplift of a rectangular area

of the sea floor spreading in one direction. By comparing our numerical results with the results obtained in [13], we observed larger normalized peak wave amplitude in the work done for the uplift of the sea floor spreading in one direction than in our work for the uplift of the sea floor spreading in two orthogonal directions which was expected due to the interaction of the velocities in the two directions.

Table 1. Values of η_{max}/ζ_0 at $v_1 = v_2 = v_t$ and h = 2 km with various values of L_1 and L_2 at $t = t_1^* = L_1/v_1$.

	L_1/h L_2/L_1			
(h = 2 km)	**0.25**	**0.5**	**0.75**	**1**
5	0.3384	0.6597	0.8115	0.8511
10	0.8359	1.2700	1.4080	1.4160
25	2.0000	2.7200	2.8300	2.8300
50	3.7220	4.6500	4.6870	4.6870
100	6.6310	7.7590	7.7640	7.7640
250	13.9200	14.920	14.920	14.920

Figure 8 represents the values of the normalized peak wave amplitude η_{max}/ζ_0 at $v_1 = v_2 = v_t$ and $h = 2$ km for different values for L_2/L_1 obtained from Table 1. It is seen how the increase in the propagation uplift length and width increases the normalized peak wave amplitude.

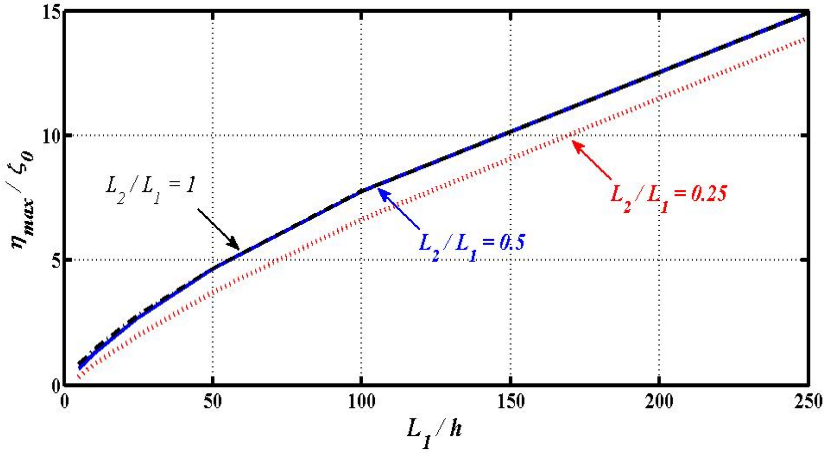

Figure 8: The normalized peak wave amplitude η_{max}/ζ_0 versus the dimensionless parameter L_1/h for $v_1 = v_2 = v_t$

3.4 Effect of water depth h on tsunami generation waveform

The effect of the water depth h on the normalized tsunami waveforms is illustrated for various values of h = 2, 4 and 6 km at constant propagated uplift length L_1 and width L_2 equal 100 km in Figure 9. It can be seen from Figure 9 that the amplitude of the normalized tsunami waveforms decreases from 4.687 m at h = 2 km to 2.099 m at h = 6 km. Hence it can be observed that maximum amplitude amplification of the normalized tsunami waveforms decrease with the increase in the water depth. This phenomenon happens because the speed of the tsunami is related to the water depth. As water depth decreases, the velocity decreases producing small wavelength and hence the height of the wave grows as the change of total energy of the tsunami remains constant. Mathematically, wave energy is proportional to both the wavelength and squared height of the wave. Therefore, if the energy remains constant and the wavelength increases, then the height must decreases. The results shown in Figure 9 for the spreading source model in two orthogonal directions agree with the aspect for the source models obtained by [10], [11] and [26] whom verified that wave amplitude is inversely proportional to water depth for uplift source models spreading in one direction.

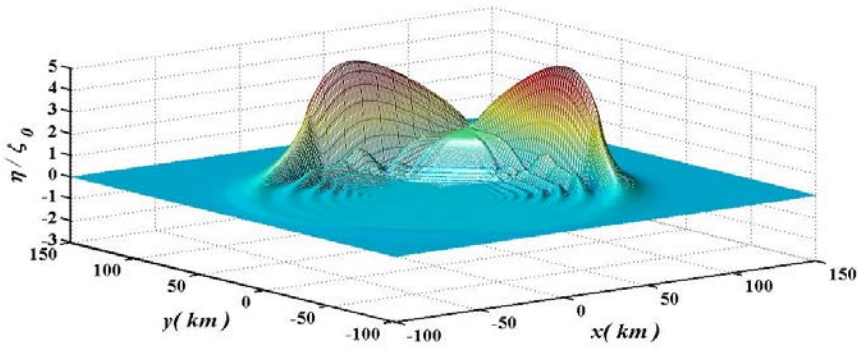

(a) h = 2 km

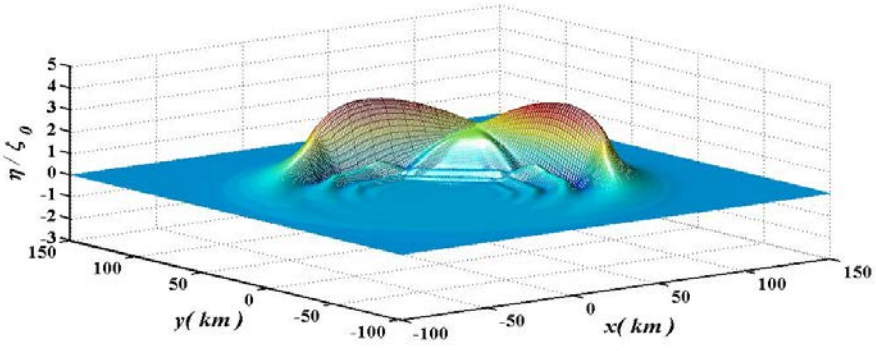

(b) h = 4 km

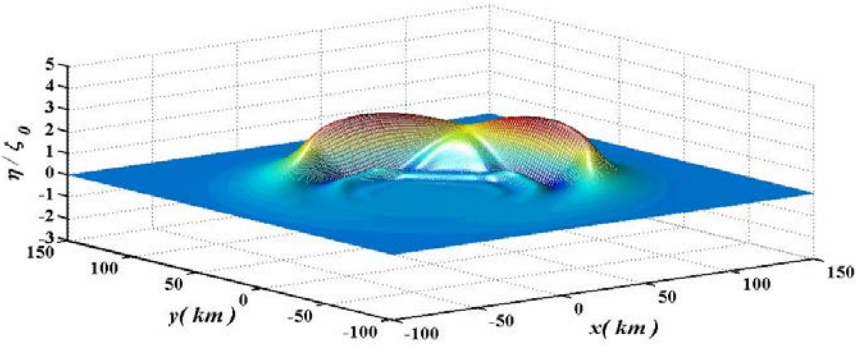

(c) h = 6 km

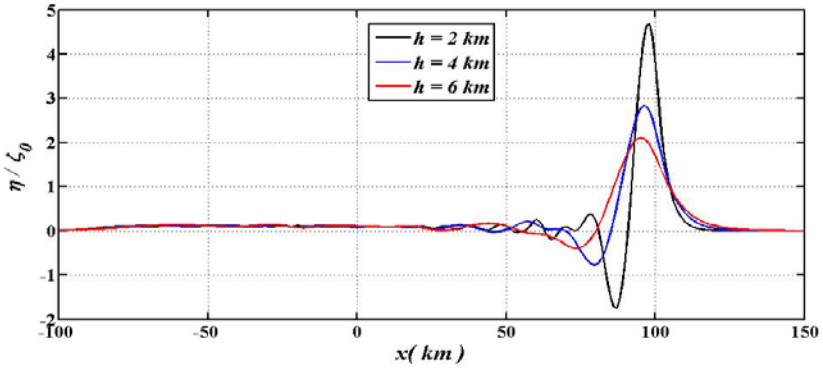

(d) Side view

Figure 9: Effect of the water depth h on the normalized tsunami generation waveforms η/ζ_0 for $L_1 = L_2 =$ 100 km and $v_1 = v_2 = v_t$ at $t = t_2^* = L_2/v_2$

Table 2 presents the effect of the water depth h on the amplification factor η_{max}/ζ_0 for various values of the ratios L_2/L_1 and at constant propagation $L_1 = 100$ km. It is seen that for h between 0.5 and 6 km, η_{max}/ζ_0 is varies from 11.66 to 2.099. The values determined in Table 2 shows that the maximum amplitude amplification decreases with the increase in h.

Table 2: Values of η_{max}/ζ_0 at $v_1 = v_2 = v_t$ and h = 2 km with various values of L_1 and L_2 at $t = t_1^* = L_1/v_1$

h (km)	**L_2/L_1**			
	0.25 0.5	**0.75**	**1.0**	
0.5	11.660	12.770	12.780	12.780
1	6.633	7.589	7.593	7.593
2	3.722	4.650	4.687	4.687
3	2.609	3.424	3.502	3.502
4	2.021	2.724	2.830	2.830
5	1.650	2.286	2.403	2.403
6	1.388	1.966	2.099	2.099

Figure 10 represents the values of the normalized peak wave amplitude η_{max}/ζ_0 at $v_1 = v_2 = v_t$ and $L_1 = 100$ km for different values for h obtained from Table 2. It is seen how the increase in the water depth h decreses the normalized peak wave amplitude.

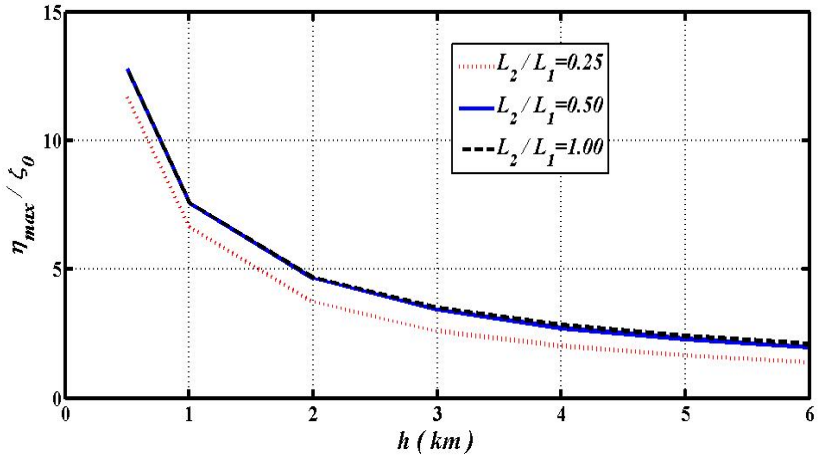

Figure 10: The normalized peak wave amplitude η_{max}/ζ_0 versus the water depth h for $v_1 = v_2 = v_t$, $L_2/L_1 \geq 0.25$ and $L_1 = 100$ km .

4. Conclusions

In this paper, the process of tsunami generation and propagation was investigated over an uplift fault source model spreading in two orthogonal directions. We studied the effect of the variation velocities of rupture propagation along the fault length and width; in the positive $x-$ and $y-$ directions with v_1 and v_2 respectively on the tsunami waveforms. It was observed that the largest peak of the tsunami amplitude at time t^* occurs when $v_1 = v_2 = v_t$ due to wave focusing. It was observed when $v_1 = v_2 = v_t$ obtained normalized peak amplitudes $\frac{\eta}{\zeta_0}$ smaller than the numerical values for one dimensional solution because of the interaction of the velocities. This phenomenon was ignored in the previous studies. Accordingly, this study might help to explain some unpredictable outcomes of tsunamis. We demonstrated the waveform amplification resulting from fault source model spreading in the $x-$ and $y-$ directions and wave focusing in the near-field and the tsunami spreading in the far-field at $v_1 = v_2 = v_t$. It was observed that near the source model, the wave has large amplitude. This amplification depends on the characteristic size of the displaced area and the time it takes to spread the motion over the entire source region. As the tsunami further departed away from the source the amplitude decreased due to dispersion. We illustrated and numerically analyzed the dependence of the peak amplification of the tsunami waveforms by changing the length of propagation, the width of the source and the water depth. It was found that the maximum amplitude amplification is proportion to the propagation length and the width of the source model and inversely proportional with the water depth. These results agreed with the aspect of the tsunami generated by the spreading uplift of the ocean bottom in one direction presented by [10, 11, 13, 26].

References

[1] Hossam S. Hassan, Khaled T. Ramadan, and Sarwat N. Hanna. 2010. " Numerical solution of the rotating shallow water flows with topography using the fractional steps method" Applied Mathematics, 1(2): pp 104–117.

[2] Ari Ben-Menahem and Martin Rosenman.1972,"Amplitude patterns of tsunami waves from submarine earthquakes" Journal of Geophysical Research, 77(17) pp. 3097–3128.

[3] E. O. Tuck and L. S. Hwang. 1972, "Long wave generation on a sloping beach" *J. Fluid Mech.*, 51:pp. 449–461.

[4] S. Tinti and E. Bortolucci. 2000,"Analytical investigation on tsunamis generated by submarine slides". Annali Di Geofisica, 43(3): pp. 519–536.

[5] D. Dutykh, F. Dias, and Y. Kervella. 2006."Linear theory of wave generation by a moving bottom". *C. R. Acad. Sci. Paris, Ser. I*, 343: pp. 499–504.

[6] M. S. Abou-Dina and F. M. Hassan. 2006,"Generation and propagation of nonlinear tsunamis in shallow water by a moving topography". Applied Mathematics and Computation, 177:pp.785–806.

[7] D. Dutykh and F. Dias."Water waves generated by a moving bottom, Tsunami and Nonlinear waves". Springer Verlag (Geo Sc.), 2007.

[8] Y. Kervella, D. Dutykh, and F. Dias. 2007 "Comparison between three-dimensional linear and nonlinear tsunami generation models". Theor. Comput. Fluid Dyn., 21: pp.245–269.

[9] F. M. Hassan. 2009"Boundary integral method applied to the propagation of non-linear gravity waves generated by a moving bottom". Applied Mathematical Modelling, 33:pp.451–466.

[10] Hossam S. Hassan, Khaled T. Ramadan, and Sarwat N. Hanna. 2010 "Generation and propagation of tsunami by a moving realistic curvilinear slide shape with variable velocities in linearized shallow-water wave theory". Engineering, 2(7): pp. 529–549.

[11] Khaled T. Ramadan, Hossam S. Hassan, and Sarwat N. Hanna.2011"Modeling of tsunami generation and propagation by a spreading curvilinear seismic faulting in linearized shallow-water wave theory". Applied Mathematical Modelling, 35(1): pp. 61–79.

[12] J. L. Hammack. 1973"A note on tsunamis: their generation and propagation in an ocean of uniform depth". J. Fluid Mech., 60:769–799.

[13] M. I. Todorovska and M. D. Trifunac.2001"Generation of tsunamis by a slowly spreading uplift of the sea floor". Soil Dynamics and Earthquake Engineering, 21: pp.151–167.

[14] M. D. Trifunac and M. I. Todorovska. 2002 "A note on differences in tsunami source parameters for submarine slides and earthquakes". Soil Dynamics and Earthquake Engineering, 22(2): pp.143 – 155.

[15] M. I. Todorovska, A. Hayir, and M. D. Trifunac. 2002 "A note on tsunami amplitudes above submarine slides and slumps". Soil Dynamics and Earthquake Engineering, 22(2): pp.129 – 141.

[16] M. D. Trifunac, A. Hayir, and M. I. Todorovska. 2002 "A note on the effects of nonuniform spreading velocity of submarine slumps and slides on the near-field tsunami amplitudes". Soil Dynamics and Earthquake Engineering, 22(3): pp.167 – 180.

[17] M. D. Trifunac, A. Hayir, and M. I. Todorovska.2002"Was grand banks event of 1929 a slump spreading in two directions". Soil Dynamics and Earthquake Engineering, 22(5): pp.349 – 360.

[18] A. Hayir. 2006 " The near-field tsunami amplitudes caused by submarine landslides and slumps spreading in two orthogonal directions". Ocean Engineering, 33: pp.654–664.

[19] V. V. Titov and F. I. Gonzalez. Implementation and testing of the method of splitting tsunami (most) model. Technical Report 1927, NOAA/Pacific Marine Environmental Laboratory, 1997.

[20] A. Yu. Bezhaev, M. M. Lavrentiev, An. G. Marchuk, and V. V. Titov. 2006"Determination of tsunami sources using deep ocean wave records". Bull. Nov.Comp. Center Math. Model in Geoph, 11: pp.53–63.

[21] D. R. Fuhrman and Per. A. Madsen. 2009"Tsunami generation, propagation, and run-up with a high-order boussinesq model". Coastal Engineering, 56: pp.747–758.

[22] Xi Zhao, B. Wang, and H. Liu. 2009."Modeling the submarine mass failure induced tsunamis by boussinesq equations". Journal of Asian Earth Sciences, 36:pp.47–55.

[23] H. Kanamori and G. S. Stewart. 1972 "A slowly earthquake". Phys. Earth Planet. Inter., 18: pp.167–175.

[24] P. G. Silver and T. H. Jordan. 1983"Total-moment spectra of fourteen large earthquakes". J. Geophys. Res., 88: pp. 3273–3293.

[25] Walter Craig. 2006 "Surface water waves and tsunamis".Journal of Dynamics and Differential Equations, 18: pp.525–549.

[26] A. Hayir. 2004 "Ocean depth effects on tsunami amplitudes used in source models in linearized shallow-water wave theory". Ocean Engineering, 31: pp. 353–361.